Solution-Processed pH-Neutral Conjugated Polyelectrolyte Improves Interfacial Contact in Organic Solar Cells

Huiqiong Zhou,† Yuan Zhang,† Cheng-Kang Mai, Jason Seifter, Thuc-Quyen Nguyen, Guillermo C. Bazan,* and Alan J. Heeger*

Center for Polymers and Organic Solids, University of California, Santa Barbara, Santa Barbara, California 93106, United States. †H.Z. and Y.Z. contributed equally to this work.

ABSTRACT The intrinsic acidic nature of poly(3,4-ethylenedioxythiophene):poly(styrenesulfonate) (PEDOT:PSS) hole-transporting layer (HTL) induces interfacial protonation and limits the device performance in organic solar cells based on basic pyridylthiadiazole units. By utilizing a pH neutral, water/alcohol soluble conjugated polyelectrolyte CPE-K as the HTL in p-DTS(PTTh$_2$)$_2$:PC$_{71}$BM solar cells, a 60% enhancement in PCE has been obtained with an increased V_{bi}, reduced R_s, and improved charge extraction. These effects originate from the elimination of interfacial protonation and energy barrier compared with the PEDOT:PSS HTL.

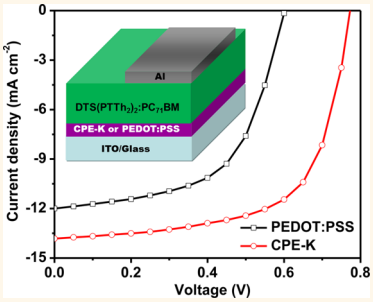

KEYWORDS: organic solar cells · bulk heterojunctions · hole-transporting layers · interface engineering · interfacial interaction

Molecular design is essential for the development of high performance optoelectronic materials in applications of organic solar cells (OSCs), organic field-effect transistors (OFETs), and organic light-emitting diodes (OLEDs).[1−5] Numerous research efforts have been devoted to understanding and utilizing the donor (D)−acceptor (A) type architecture for organic semiconductors to enable versatile and tunable optoelectronic properties.[1,2,6,7] Recently, the pyridyl[2,1,3]thiadiazole (PT) moiety has been incorporated as an electron poor moiety in molecular designs with a D−A type architecture.[1,8−10] Narrow band-gaps with deep HOMO levels can be achieved as a result of intramolecular charge transfer from the electron rich fragment (D) to the electron deficient PT segment (A), which decreases both the HOMO and LUMO levels simultaneously. These π-conjugated materials containing PT units have shown an impressive hole mobility up to 50 cm^2 V^{-1} s^{-1} in OFETs,[10,11] and high power conversion efficiencies (PCEs) in solution-processed small molecule[12−16] and polymer bulk-heterojunction (BHJ) solar cells.[1,17] Organic BHJ solar cells have been studied extensively due to their unique advantages, such as low cost, lightweight, and flexibility.[18,19] In solar cells, the unique feature of PT units containing basic pyridyl nitrogen tends to induce the chemical interaction between the interface of the basic PT unit and the acidic poly(3,4-ethylenedioxythiophene): poly(styrenesulfonate) (PEDOT:PSS), which is commonly used as a hole transporting layer (HTL). For example, the device performance of solar cells based on the small molecule donor, 5,5′-bis{(4-(7-hexylthiophen-2-yl)thiophen-2-yl)-[1,2,5]thiadiazolo[3,4-*c*]pyridine}-3,3′-di-2-ethylhexylsilylene-2,2′-bithiophene (DTS(PTTh$_2$)$_2$, molecular structure shown in the inset in Figure 1a), has been restricted by the protonation of PT units when using PEDOT:PSS HTLs.[16,20,21] Thus, a pH neutral HTL is preferred to avoid the interfacial chemical reactions. Alternatively, metal oxides such as MoO_x[14] and NiO_x,[20,21] have been utilized to improve the interfacial contact in small molecule p-DTS(PTTh$_2$)$_2$ solar cells. However, fill factors (FFs) in those solar cells remain far from optimized (below 60%),

* Address correspondence to bazan@chem.ucsb.edu, ajhe1@physics.ucsb.edu.

Received for review September 22, 2014 and accepted December 15, 2014.

Published online December 15, 2014
10.1021/nn505378m

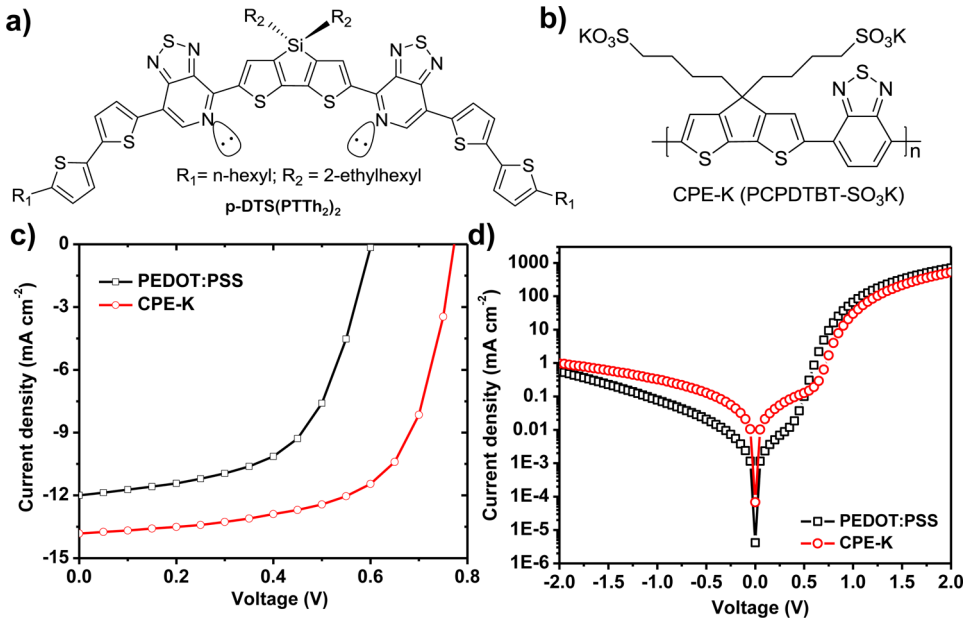

Figure 1. Molecular structures of (a) p-DTS($PTTh_2$)$_2$ and (b) conjugated polyelectrolyte CPE-K (PCPDTBT-SO_3K). Current density (J)−voltage (V) characteristics of p-DTS($PTTh_2$)$_2$:$PC_{71}BM$ solar cells using PEDOT:PSS and CPE-K HTLs when measured (c) under irradiation and (d) in dark.

which indicates that the interface between p-DTS($PTTh_2$)$_2$ active layers and metal oxides hole-transporting layer can further be improved.

In this work, we study effects of the interfacial contact on the device performance and device physics in small molecule BHJ solar cells based on p-DTS($PTTh_2$)$_2$ as the electron donor and [6,6]-phenyl C71-butyric acid methyl ester ($PC_{71}BM$) as the acceptor. A unique water/alcohol soluble conjugated polyelectrolyte (CPE), poly[2,6-(4,4-bis-potassiumbutanylsulfonate-4*H*-cyclopenta-[2,1-b;3,4-b′]-dithiophene)-*alt*-4,7-(2,1,3-benzothiadiazole)] (CPE-K,[22] molecular structure shown in Figure 1b), was utilized instead of commercial PEDOT:PSS as a HTL. CPE-K is pH neutral and solution processable. It has an appropriate work function and sufficiently high electrical conductivity, to be a suitable candidate for a hole transporting material.[23] Importantly, the interfacial protonation of pyridyl nitrogen between CPE-K HTLs and BHJ active layers has been eliminated, as confirmed by X-ray photoemission spectroscopy (XPS), ultraviolet photoemission spectroscopy (UPS) and impedance measurements. The device performance shows a 60% enhancement in PCEs when the PEDOT:PSS HTL is replaced by a CPE-K HTL, with a simultaneous improvement in the short circuit current (J_{sc}), open circuit voltage (V_{oc}), and fill factor.

RESULTS AND DISCUSSION

Device Performance. Typical current density *versus* voltage (J−V) characteristics of p-DTS($PTTh_2$)$_2$:$PC_{71}BM$ solar cells with PEDOT:PSS and CPE-K HTLs under 1000 W m^{-2} air mass 1.5 global (AM 1.5 G) illumination are shown in Figure 1c. A PCE of 4.2% is achieved in optimized devices using a PEDOT:PSS HTL. The replacement of PEDOT:PSS by CPE-K leads to a significant enhancement in PCE up to 6.8% with simultaneously improved V_{oc} (from 0.60 ± 0.02 V to 0.77 ± 0.01 V), J_{sc} (from 11.99 ± 0.23 mA cm^{-2} to 13.81 ± 0.21 mA cm^{-2}) and FF (from 57.9 ± 0.11% to 63.8 ± 0.12%). The external quantum efficiency (EQE) spectra are shown in Figure S1 (Supporting Information). We observe an increase of EQE over the whole absorption spectrum (350−750 nm) for the CPE-K device in comparison to the PEDOT:PSS device. This indicates that CPE-K is superior to PEDOT:PSS as a HTL for charge collection in p-DTS($PTTh_2$)$_2$:$PC_{71}BM$ solar cells. Under illumination, the CPE-K device shows a V_{oc} of 0.77 V, approximately 150 mV higher than the PEDOT:PSS device with a V_{oc} = 0.60 V. The J−V characteristics in dark of the CPE-K device exhibits a higher built-in voltage (V_{bi}), estimated from the voltage that starts to deviate from the diffusion current. The V_{bi} of the CPE-K cell is around 0.95 V, 150 mV higher that that estimated on the PEDOT:PSS device (see Figure 1d). The V_{bi} provides an upper limit for the V_{oc} and strongly influences the internal electric field in organic BHJ solar cells.[24] Thus, the increase of V_{bi} may be responsible for the increase of V_{oc} in the CPE-K device compared with PEDOT:PSS devices.

Interface Characterization. Figure S2c,d compare the surface morphology of p-DTS($PTTh_2$)$_2$:$PC_{71}BM$ films on PEDOT:PSS (Figures S2a) and CPE-K HTLs (Figures S2b) examined by atomic force microscopy (AFM). The p-DTS($PTTh_2$)$_2$:$PC_{71}BM$ film on PEDOT:PSS exhibits a homogeneous surface with a root-mean-square (rms) roughness of 0.97 nm. The p-DTS($PTTh_2$)$_2$:$PC_{71}BM$ film on CPE-K shows no obvious change in the film

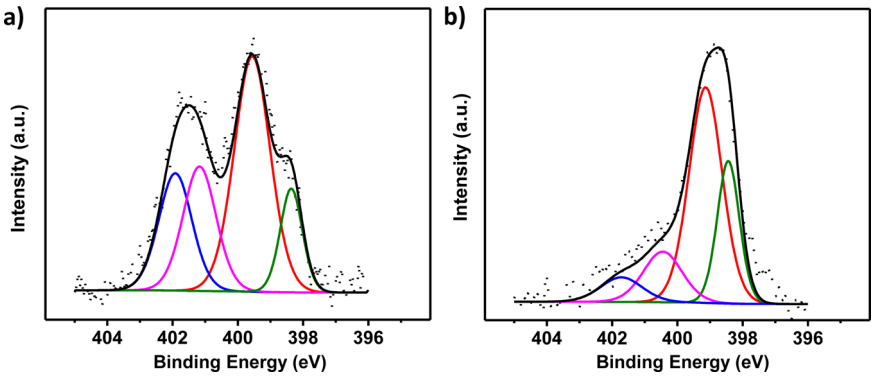

Figure 2. XPS of core level N 1s of p-DTS($PTTh_2$)$_2$ at the interface between p-DTS($PTTh_2$)$_2$:$PC_{71}BM$ BHJ layers and HTLs of (a) PEDOT:PSS and (b) CPE-K.

morphology and surface roughness. XRD[25] results from out of plane (Figure S2c) and in plane (Figure S2d) measurements show similar spectra of p-DTS($PTTh_2$)$_2$:$PC_{71}BM$ films when cast on PEDOT:PSS and CPE-K HTLs.[26,27] Hence, the effect of the two different HTLs on the crystallinity of p-DTS($PTTh_2$)$_2$:$PC_{71}BM$ BHJ is negligible. These results suggest that the enhancement of device characteristics in CPE-K devices may originate from the intrinsic properties of HTLs and the interface between HTLs and BHJ active layers. It has been demonstrated in a previous work that CPE-K as a HTL can provide comparable PCEs in both small molecule and polymer cells, owing to a similar optical transparency and a higher out-of-plane electrical conductivity when compared to PEDOT:PSS.[23] In the current case, the enhancement in the device performance of p-DTS($PTTh_2$)$_2$:$PC_{71}BM$ cells indicates that the interface between pH neutral CPE-K and p-DTS($PTTh_2$)$_2$:$PC_{71}BM$ is significantly modified; a result which is reasonably attributed to the suppression of protonation in the absence of acidic functionalities.

To clarify the chemical interaction between p-DTS($PTTh_2$)$_2$ BHJ layers and HTLs, XPS measurements were carried out on the core level nitrogen at the p-DTS($PTTh_2$)$_2$:$PC_{71}BM$/HTL interfaces, which were made accessible through floating off the p-DTS($PTTh_2$)$_2$:$PC_{71}BM$ active layer from the ITO/HTL substrates by dissolving CPE-K or PEDOT:PSS in deionized water. Figure S3a shows the N 1s spectrum for the pure p-DTS($PTTh_2$)$_2$ on an inert Au surface. The two chemically different nitrogen atoms in the pyridyl cycle at 397.9 eV and the thiadiazole unit at 399.1 eV[28] can be clearly separated by a peak-fitting routine using two components. The intensity ratio of the thiadiazole to pyridyl components is in good agreement with the expected stoichiometry at 2:1. The N 1s spectrum at the p-DTS($PTTh_2$)$_2$:$PC_{71}BM$/PEDOT:PSS interface shows an additional shoulder on the high binding energy side (Figure 2a), resulting from the protonation of the pyridyl nitrogen in p-DTS($PTTh_2$)$_2$. The high binding energy components at 401.2 eV (pyridyl) and 401.9 eV (thiadiazole) can be fitted for the protonated p-DTS($PTTh_2$)$_2$.[20,21] On the contrary, the intensity of high binding energy components is dramatically decreased in the spectrum at the p-DTS($PTTh_2$)$_2$:$PC_{71}BM$/CPE-K interface (Figure 2b). This is indicative that the protonation of p-DTS($PTTh_2$)$_2$ at the interface is efficiently suppressed. The tail to the high binding energy in this N 1s peak may stem from the signal of self-protonated thiadiazole nitrogens in CPE-K (Figure S3b)[22] because protonation is unlikely to occur between p-DTS($PTTh_2$)$_2$ and CPE-K with a pH value of 7.56. The spectra attained at the top surface of p-DTS($PTTh_2$)$_2$:$PC_{71}BM$ BHJ layers when cast on PEDOT:PSS and CPE-K (Figure S3c,d) show a similar feature with that of p-DTS($PTTh_2$)$_2$ deposited on Au. The absence of protonation peaks indicate that in the solar cell, protonation only occurs at the interface of BHJ layers and HTLs.

To enable a more in-depth understanding of the electronic structure at the interface near the anode,[29] UPS measurements (Figure 3a,b) were performed on p-DTS($PTTh_2$)$_2$ films deposited on PEDOT:PSS and CPE-K as a function of active layer film thickness, adjusted by solution concentrations. Figure 3c,d show the energy diagrams of p-DTS($PTTh_2$)$_2$/PEDOT:PSS and p-DTS($PTTh_2$)$_2$/CPE-K interfaces analyzed based on the UPS spectra in Figure 3a,b. In Figure 3a, the spectrum on the bottom is obtained on a clean PEDOT:PSS surface with an ionization potential (IP) of 5.1 eV, as determined by the incident photon energy ($h\nu$ = 21.2 eV) for HeI, E_{cutoff} at the higher binding energy side (left panel), and E_{HOMO} at the lower binding energy side (right panel) by using the equation IP = $h\nu$ − (E_{cutoff} − E_{HOMO}).[25,30] The E_{cutoff} corresponds to the vacuum level of the film, depending on the film thickness. The UPS spectrum of the lowest concentration p-DTS($PTTh_2$)$_2$ displays a local vacuum level shift toward the lower binding energy side. This provides evidence of forming a weak dipole between the p-DTS($PTTh_2$)$_2$ and PEDOT:PSS. With increasing the thickness, the contribution from p-DTS($PTTh_2$)$_2$ to the UPS signal becomes more dominant, as shown in the top spectrum. In this situation, the UPS spectrum is dictated by the intrinsic

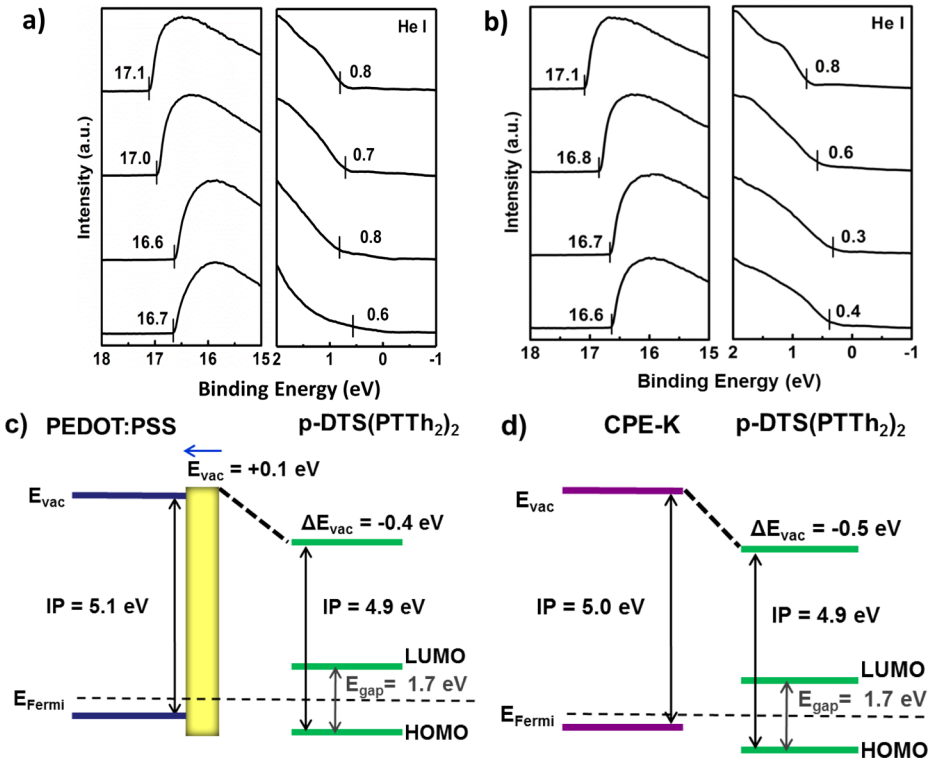

Figure 3. UPS spectra of p-DTS(PTTh$_2$)$_2$ on (a) PEDOT:PSS and (b) CPE-K. From top to bottom are films of p-DTS(PTTh$_2$)$_2$ prepared from a 3, 0.5, 0.1, and 0 mg/mL solution. Interfacial energy diagrams of (c) p-DTS(PTTh$_2$)$_2$/PEDOT:PSS and (d) p-DTS(PTTh$_2$)$_2$/CPE-K interfaces obtained from the UPS results.

electronic structure of p-DTS(PTTh$_2$)$_2$. Consistently, the vacuum level of PEDOT:PSS first increases by ~0.1 eV along a few nanometers within the interface and then decreases toward the vacuum level of p-DTS(PTTh$_2$)$_2$ as the film thickness increases (Figure 3c), which may indicate an interfacial energy barrier formed at the p-DTS(PTTh$_2$)$_2$/PEDOT:PSS interface.[21] In contrast, the energy diagram of the p-DTS(PTTh$_2$)$_2$/CPE-K interface in Figure 3b,d shows a monotonic decrease in the vacuum level of CPE-K toward the vacuum level of p-DTS(PTTh$_2$)$_2$ as the film thickness increases. This result suggests that there are no corresponding interactions or energy barrier at the p-DTS(PTTh$_2$)$_2$/CPE-K interface. Consequently, dissociated charges can be more efficiently extracted in solar cells with CPE-K HTL.

Impedance Measurement. These differences in interfaces can directly influence the contact properties and resultant V_{bi} in solar cells. To probe these parameters, we performed capacitance (C)−voltage (V) measurements and AC impedance measurements of p-DTS(PTTh$_2$)$_2$:PC$_{71}$BM solar cells containing PEDOT:PSS and CPE-K HTLs. The V_{bi} is estimated by the voltage corresponding to the maximal capacitance which equals the flat-band condition. Because of the lack of a well-defined depletion regime and Schottky contact, the flat-band voltage can serve as a sound approximation of the V_{bi}.[31] The $C-V$ characteristics shown in Figure 4a were attained by applying a low AC perturbation signal by sweeping the DC bias under a fixed frequency. A V_{bi} = 0.85 V for the device with PEDOT:PSS HTL and a V_{bi} = 0.94 V for the device with CPE-K HTL were obtained. These values are consistent with the results estimated from dark $J-V$ characteristics in Figure 3d. The increase of V_{bi} is attributed to the eliminated energy barrier, leading to a higher V_{oc} in p-DTS(PTTh$_2$)$_2$:PC$_{71}$BM devices with CPE-K HTLs.

Figure 4b shows Nyquist plots of the impedance of p-DTS(PTTh$_2$)$_2$:PC$_{71}$BM devices using PEDOT:PSS or CPE-K HTLs with the frequency swept from 500 Hz to 1 MHz. The data were fit by using equivalent circuit modeling (ECM) with detailed circuits depicted in Figure S4.[32] For the CPE-K device, an ECM consisting of a double RC in parallel connection (Model I) was applied, where the two capacitors stand for the depletion ($C_{surface}$) and bulk capacitance (C_{bulk}), respectively. As a result, the ECM yields satisfactory agreement with the measurements. In contrast, Model I cannot be satisfactorily applied for the PEDOT:PSS device. We added an extra RC component connected in parallel with the depletion capacitance to improve the data modeling (Figure S4, Model II).[33] This additional RC component can be ascribed to interfacial traps resulting from protonation. With CPE-K HTLs, the suppression of protonation can lead to the passivation of interfacial traps.[34] This is in line with the results of XPS and UPS measurements as mentioned above. The series resistance (R_s) of solar cells under the operational

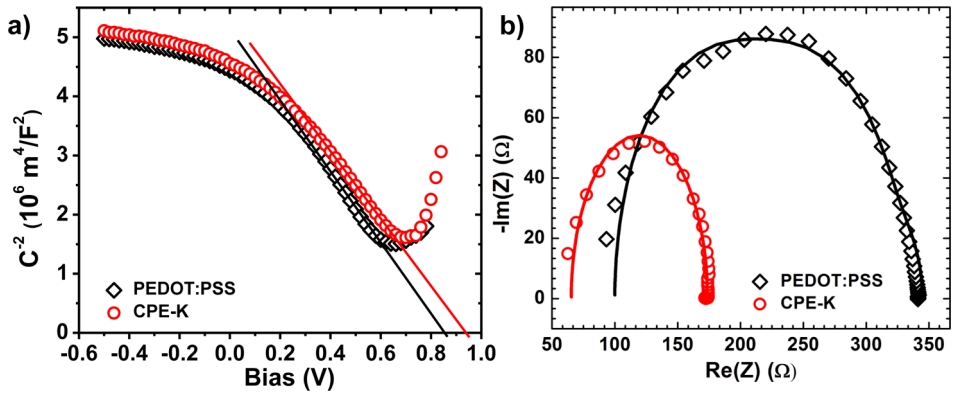

Figure 4. (a) C^{-2} *versus* bias characteristics of solar cells measured in dark. The solid lines are linear fittings used for Mott−Schottky analysis. (b) Niquist plots of impedance analysis. The data are fitted by the equivalent circuit model I and II for CPE-K and PEDOT:PSS devices, respectively (see models in Supporting Information).

condition is obtained from extrapolating ReZ to high frequencies (left part) in the Nyquist plots. When replacing PEDOT:PSS by CPE-K, R_s is reduced from 4.5 Ω cm^2 to 2.7 Ω cm^2 in p-DTS($PTTh_2$)$_2$:$PC_{71}BM$ solar cells, which benefits the improvement in J_{sc} and FF. The reduced R_s is also well correlated to the higher out-of-plane electrical conductivity of CPE-K.

Charge Extraction. We further investigate the influences of HTLs on the hole extraction by hole-only diode measurements based on p-DTS($PTTh_2$)$_2$:$PC_{71}BM$ blends using a structure of ITO/HTLs/p-DTS($PTTh_2$)$_2$:$PC_{71}BM$/Au. The $J-V$ characteristics were fit by the Mott−Gurney law (the space-charge limited current model, SCLC),[35−37]

$$J = 9\varepsilon_r\varepsilon_0\mu(V - V_{bi})^2/8L^3 \quad (1)$$

where $\varepsilon_r\varepsilon_0$ is the dielectric constant of the active layer, μ is the mobility, and L is the thickness of the active layer. As shown in Figure 5, the hole current of the device with PEDOT:PSS (plotted in a double log scale) shows a limited range of quadratic voltage dependence and displays a stronger bias dependence, particularly at higher bias. This feature is consistent with the formation of injection limited current. We estimate the *effective* hole mobility by applying the SCLC model, yielding an effective mobility of 1.2 × 10^{-7} cm^2 V^{-1} s^{-1}. With the hole injection barrier confirmed by UPS, the determined hole mobility should be contact-limited and thus cannot directly reflect the bulk transport properties in p-DTS($PTTh_2$)$_2$:$PC_{71}BM$. In the CPE-K device, the hole current is much higher than that of the PEDOT:PSS device based on the same thickness of active layers. Importantly the current voltage characteristic exhibits a large range of quadratic dependence. By using the SCLC model, we attain a hole mobility of 1.5 × 10^{-5} cm^2 V^{-1} s^{-1}, an enhancement of nearly 2 orders of magnitude due to achieving an Ohmic interfacial contact between CPE-K and p-DTS($PTTh_2$)$_2$:$PC_{71}BM$ active layer. With the improved hole extraction, more balanced charge transport in the solar cell

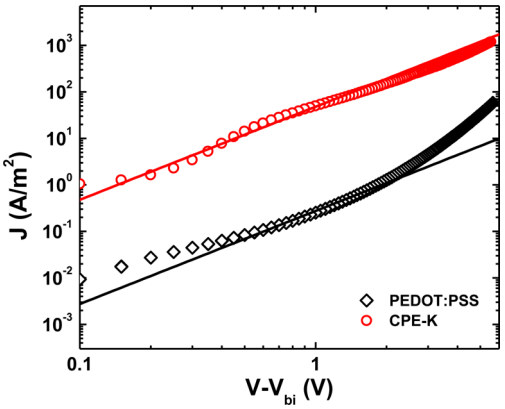

Figure 5. $J-V$ characteristics of hole-only devices using a configuration of ITO/CPE-K (or PEDOT:PSS)/active layer/Au. The solid lines represent the best fitting with the SCLC model.

with CPE-K is achieved. This can lead to increased J_{sc} and FF in CPE-K devices by restricting the buildup of space charges, such that charge recombination is effectively reduced.[38]

CONCLUSION

In conclusion, a pH neutral conjugated polyelectrolyte CPE-K has been successfully applied for hole transporting layers in p-DTS($PTTh_2$)$_2$:$PC_{71}BM$ BHJ solar cells. A 60% enhancement in device efficiency has been achieved when compared with devices using PEDOT:PSS HTL. The increased built-in voltage of the device using CPE-K HTLs results in a larger open-circuit voltage, which is due to the elimination of an interfacial phenomena by obviating protonation of the basic PT group in p-DTS($PTTh_2$)$_2$ at the interface between the HTL and the BHJ active layer. The decrease in series resistance and the enhancement of hole extraction capability lead to improving the short-circuit current density and fill factor in CPE-K solar cells. These results not only demonstrate the possibility of incorporating a pH neutral conjugated polyelectrolyte to enhance the

solar cell performance based on donor materials with Lewis basic functionalities, but also provide insights into the effect of interfacial interactions on device performance and device physics.

METHODS

Device Fabrication. DTS(PTTh$_2$)$_2$ (p-DTS(PTTh$_2$)$_2$) was purchased from 1-Material Chemscitech Inc. (St-Laurent, Quebec, Canada) and used as received. Detailed synthesis of CPE-K was reported elsewhere. The device structure was ITO/PEDOT:PSS-(or CPE-K)/p-DTS(PTTh$_2$)$_2$:PC$_{71}$BM/Al. A thin layer (~30 nm) of PEDOT:PSS (Baytron PVP Al 4083) was spin-coated onto a cleaned ITO surface and annealed in air at 140 for 10 min. Then, blend films of p-DTS(PTTh$_2$)$_2$:PC$_{71}$BM were cast from a solution with concentration of 40 mg/mL and p-DTS(PTTh$_2$)$_2$:PC$_{71}$BM ratio of 7:3 in chlorobenzene/1,8-diiodoctane (0.25 vol %) mixed solvent at 2000 rpm for 40 s. CPE-K was dissolved in water/methanol mixture solvent with concentration of 5 mg/mL and the fabrication of CPE-K HTL was similar to that for PEDOT:PSS. The devices were completed after deposition of 100 nm Al as cathode (4.5 mm^2). Devices were encapsulated for testing in air with a UV-curable epoxy and covered with a glass slide.

Characterization and Measurement. Current density−voltage ($J-V$) characteristics of the devices were measured by a Keithley 2400 Source Measure Unit, and a Newport Air Mass 1.5 Global (AM 1.5G) full spectrum solar simulator with an irradiation intensity of 100 mW cm^{-2}. In all cases a circular aperture (3.98 mm^2) was used for obtaining the current−voltage curves. The 100 mW cm^{-2} spectrum of incident light was spectrum and intensity matched with an Ocean Optics USB4000 spectrometer calibration standard lamp with NIST-traceable calibration from 350 to 1000 nm. External quantum efficiency (EQE) spectra were measured using a 75 W Xe lamp, Newport monochromator, Newport optical chopper, and a Stanford Research Systems lock-in amplifier. Power-density calibration was done with a National Institute of Standards and Technology traceable silicon photodiode.

The XPS and UPS measurements were performed in a Kratos Ultra spectrometer (base pressure of 1 × 10−9 Torr) using monochromatized Al Kα X-ray photons (hv = 1486.6 eV f or XPS) and a HeI (21.2 eV for UPS) discharge lamp. The capacitance−voltage measurement and the AC impedance measurements were conducted using an Agilent 4192A impedance analyzer. The AC impedance measurements were done in $Z-\theta$ mode by varying the frequency (f) from 500 Hz to 1 MHz, and a fixed AC drive bias of 25 mV. A constant DC bias equal to the open-circuit voltage of the solar cell device was applied, superimposed on the AC bias. SCLC measurements for p-DTS(PTTh$_2$)$_2$:PC$_{71}$BM devices were explored in configuration of ITO/CPE-K (or PEDOT:PSS) /active layer/Au for hole-only device.

Conflict of Interest: The authors declare no competing financial interest.

Acknowledgment. This work is supported by the Department of Energy Office of Basic Energy Sciences (DE-FG02-08ER46535). We thank Dr. David Wynands and Dr. Chris Takacs for helpful discussions. We thank Air Force Office of Scientific Research (AFOSR MURI FA9550-12-1-0002) for supporting the synthesis of CPE-K and the NSF (DMR-1121053) for providing the XPS instrumentation. A.J.H., G.C.B. and T.Q.N supervised the project and participated in the writing the manuscript. H.Z. and Y.Z. initiated the experimental plan and wrote the initial manuscript. H.Z. fabricated solar cell devices and performed XPS/UPS measurements. Y.Z. performed hole-only diode and impedance measurements. C.K.M. synthesized the CPE-K. J.S. carried out AFM and XRD measurements.

Supporting Information Available: EQE spectra of p-DTS-(PTTh$_2$)$_2$:PC$_{71}$BM solar cells using different HTLs, AFM images of different HTLs and BHJ layers on different HTLs, XRD spectra of BHJ layers on different HTLs, XPS spectra, equivalent circuit models for impedance measurements, device performance comparation of p-DTS(PTTh$_2$)$_2$:PC$_{71}$BM using different HTLs. This material is available free of charge *via* the Internet at http://pubs.acs.org.

REFERENCES AND NOTES

1. Blouin, N.; Michaud, A.; Gendron, D.; Wakim, S.; Blair, E.; Neagu-Plesu, R.; Belletete, M.; Durocher, G.; Tao, Y.; Leclerc, M. Toward a Rational Design of Poly(2,7-Carbazole) Derivatives for Solar Cells. *J. Am. Chem. Soc.* **2008**, *130*, 732–742.
2. Henson, Z. B.; Mullen, K.; Bazan, G. C. Design Strategies for Organic Semiconductors beyond the Molecular Formula. *Nat. Chem.* **2012**, *4*, 699–704.
3. Thompson, B. C.; Frechet, J. M. J. Organic Photovoltaics—Polymer-Fullerene Composite Solar Cells. *Angew. Chem., Int. Ed.* **2008**, *47*, 58–77.
4. Lu, L.; Yu, L. Understanding Low Bandgap Polymer PTB7 and Optimizing Polymer Solar Cells Based on It. *Adv. Mater.* **2014**, *26*, 4413–4430.
5. Wu, W. P.; Liu, Y. Q.; Zhu, D. B. pi-Conjugated Molecules with Fused Rings for Organic Field-Effect Transistors: Design, Synthesis and Applications. *Chem. Soc. Rev.* **2010**, *39*, 1489–1502.
6. Guo, X.; Zhou, N.; Lou, S. J.; Smith, J.; Tice, D. B.; Hennek, J. W.; Ortiz, R. P.; Navarrete, J. T. L.; Li, S.; Strzalka, J.; Chen, L. X.; Chang, R. P. H.; Facchetti, A.; Marks, T. J. Polymer Solar Cells with Enhanced Fill Factors. *Nat. Photonics* **2013**, *7*, 825–833.
7. Liang, Y. Y.; Xu, Z.; Xia, J. B.; Tsai, S. T.; Wu, Y.; Li, G.; Ray, C.; Yu, L. P. For the Bright Future-Bulk Heterojunction Polymer Solar Cells with Power Conversion Efficiency of 7.4%. *Adv. Mater.* **2010**, *22*, E135–E138.
8. Henson, Z. B.; Welch, G. C.; van der Poll, T.; Bazan, G. C. Pyridalthiadiazole-Based Narrow Band Gap Chromophores. *J. Am. Chem. Soc.* **2012**, *134*, 3766–3779.
9. Welch, G. C.; Bazan, G. C. Lewis Acid Adducts of Narrow Band Gap Conjugated Polymers. *J. Am. Chem. Soc.* **2011**, *133*, 4632–4644.
10. Ying, L.; Hsu, B. B. Y.; Zhan, H. M.; Welch, G. C.; Zalar, P.; Perez, L. A.; Kramer, E. J.; Nguyen, T. Q.; Heeger, A. J.; Wong, W. Y.; Bazan, G. C. Regioregular Pyridal[2,1,3]thiadiazole pi-Conjugated Copolymers. *J. Am. Chem. Soc.* **2011**, *133*, 18538–18541.
11. Luo, C.; Kyaw, A. K. K.; Perez, L. A.; Patel, S.; Wang, M.; Grimm, B.; Bazan, G. C.; Kramer, E. J.; Heeger, A. J. General Strategy for Self-Assembly of Highly Oriented Nanocrystalline Semiconducting Polymers with High Mobility. *Nano Lett.* **2014**, *14*, 2764–2771.
12. Liu, X. F.; Su, Y. M.; Perez, L. A.; Wen, W.; Toney, M. F.; Heeger, A. J.; Bazan, G. C. Narrow-Band-Gap Conjugated Chromophores with Extended Molecular Lengths. *J. Am. Chem. Soc.* **2012**, *134*, 20609–20612.
13. Steinberger, S.; Mishra, A.; Reinold, E.; Levichkov, J.; Uhrich, C.; Pfeiffer, M.; Bauerle, P. Vacuum-Processed Small Molecule Solar Cells Based on Terminal Acceptor-Substituted Low-Band Gap Oligothiophenes. *Chem. Commun.* **2011**, *47*, 1982–1984.
14. Sun, Y. M.; Welch, G. C.; Leong, W. L.; Takacs, C. J.; Bazan, G. C.; Heeger, A. J. Solution-Processed Small-Molecule Solar Cells with 6.7% Efficiency. *Nat. Mater.* **2012**, *11*, 44–48.
15. Takacs, C. J.; Sun, Y. M.; Welch, G. C.; Perez, L. A.; Liu, X. F.; Wen, W.; Bazan, G. C.; Heeger, A. J. Solar Cell Efficiency, Self-Assembly, and Dipole-Dipole Interactions of Isomorphic Narrow-Band-Gap Molecules. *J. Am. Chem. Soc.* **2012**, *134*, 16597–16606.
16. Welch, G. C.; Perez, L. A.; Hoven, C. V.; Zhang, Y.; Dang, X. D.; Sharenko, A.; Toney, M. F.; Kramer, E. J.; Nguyen, T. Q.;

Bazan, G. C. A Modular Molecular Framework for Utility in Small-Molecule Solution-Processed Organic Photovoltaic Devices. *J. Mater. Chem.* **2011**, *21*, 12700–12709.
17. Zhou, H. X.; Yang, L. Q.; Price, S. C.; Knight, K. J.; You, W. Enhanced Photovoltaic Performance of Low-Bandgap Polymers with Deep LUMO Levels. *Angew. Chem., Int. Ed.* **2010**, *49*, 7992–7995.
18. Darling, S. B.; You, F. Q. The Case for Organic Photovoltaics. *RSC Adv.* **2013**, *3*, 17633–17648.
19. Yu, G.; Gao, J.; Hummelen, J. C.; Wudl, F.; Heeger, A. J. Polymer Photovoltaic Cells—Enhanced Efficiencies *via* a Network of Internal Donor-Acceptor Heterojunctions. *Science* **1995**, *270*, 1789–1791.
20. Garcia, A.; Welch, G. C.; Ratcliff, E. L.; Ginley, D. S.; Bazan, G. C.; Olson, D. C. Improvement of Interfacial Contacts for New Small-Molecule Bulk-Heterojunction Organic Photovoltaics. *Adv. Mater.* **2012**, *24*, 5368–5373.
21. Ratcliff, E. L.; Bakus, R. C.; Welch, G. C.; van der Poll, T. S.; Garcia, A.; Cowan, S. R.; MacLeod, B. A.; Ginley, D. S.; Bazan, G. C.; Olson, D. C. Formation of Interfacial Traps upon Surface Protonation in Small Molecule Solution Processed Bulk Heterojunctions Probed by Photoelectron Spectroscopy. *J. Mater. Chem. C* **2013**, *1*, 6223–6234.
22. Mai, C. K.; Zhou, H. Q.; Zhang, Y.; Henson, Z. B.; Nguyen, T. Q.; Heeger, A. J.; Bazan, G. C. Facile Doping of Anionic Narrow-Band-Gap Conjugated Polyelectrolytes During Dialysis. *Angew. Chem., Int. Ed.* **2013**, *52*, 12874–12878.
23. Zhou, H.; Zhang, Y.; Mai, C.-K.; Collins, S. D.; Nguyen, T.-Q.; Bazan, G. C.; Heeger, A. J. Conductive Conjugated Polyelectrolyte As Hole-Transporting Layer for Organic Bulk Heterojunction Solar Cells. *Adv. Mater.* **2014**, *26*, 780–785.
24. Brabec, C. J.; Cravino, A.; Meissner, D.; Sariciftci, N. S.; Fromherz, T.; Rispens, M. T.; Sanchez, L.; Hummelen, J. C. Origin of the Open Circuit Voltage of Plastic Solar Cells. *Adv. Funct. Mater.* **2001**, *11*, 374–380.
25. Seo, J. H.; Gutacker, A.; Sun, Y. M.; Wu, H. B.; Huang, F.; Cao, Y.; Scherf, U.; Heeger, A. J.; Bazan, G. C. Improved High-Efficiency Organic Solar Cells *via* Incorporation of a Conjugated Polyelectrolyte Interlayer. *J. Am. Chem. Soc.* **2011**, *133*, 8416–8419.
26. Jasieniak, J. J.; Hsu, B. B. Y.; Takacs, C. J.; Welch, G. C.; Bazan, G. C.; Moses, D.; Heeger, A. J. Insights into π-Conjugated Small Molecule Neat Films and Blends As Determined Through Photoconductivity. *ACS Nano* **2012**, *6*, 8735–8745.
27. Chen, W.; Nikiforov, M. P.; Darling, S. B. Morphology Characterization in Organic and Hybrid Solar Cells. *Energy Environ. Sci.* **2012**, *5*, 8045–8074.
28. Aygul, U.; Peisert, H.; Frisch, J.; Vollmer, A.; Koch, N.; Chasse, T. Electronic Properties of Interfaces between PCPDTBT and Prototypical Electrodes Studied by Photoemission Spectroscopy. *ChemPhysChem* **2011**, *12*, 2345–2351.
29. Ishii, H.; Sugiyama, K.; Ito, E.; Seki, K. Energy Level Alignment and Interfacial Electronic Structures at Organic Metal and Organic Organic Interfaces. *Adv. Mater.* **1999**, *11*, 605–625.
30. Tengstedt, C.; Osikowicz, W.; Salaneck, W. R.; Parker, I. D.; Hsu, C. H.; Fahlman, M. Fermi-Level Pinning at Conjugated Polymer Interfaces. *Appl. Phys. Lett.* **2006**, *88*, 053502.
31. Kirchartz, T.; Gong, W.; Hawks, S. A.; Agostinelli, T.; MacKenzie, R. C. I.; Yang, Y.; Nelson, J. Sensitivity of the Mott-Schottky Analysis in Organic Solar Cells. *J. Phys. Chem. C* **2012**, *116*, 7672–7680.
32. Zhang, Y.; Dang, X. D.; Kim, C.; Nguyen, T. Q. Effect of Charge Recombination on the Fill Factor of Small Molecule Bulk Heterojunction Solar Cells. *Adv. Energy Mater.* **2011**, *1*, 610–617.
33. Zhou, H. Q.; Zhang, Y.; Seifter, J.; Collins, S. D.; Luo, C.; Bazan, G. C.; Nguyen, T. Q.; Heeger, A. J. High-Efficiency Polymer Solar Cells Enhanced by Solvent Treatment. *Adv. Mater.* **2013**, *25*, 1646–1652.
34. Leong, W. L.; Cowan, S. R.; Heeger, A. J. Differential Resistance Analysis of Charge Carrier Losses in Organic Bulk Heterojunction Solar Cells: Observing the Transition from Bimolecular to Trap-Assisted Recombination and Quantifying the Order of Recombination. *Adv. Energy Mater.* **2011**, *1*, 517–522.
35. Zhang, Y.; Blom, P. W. M. Enhancement of the Hole Injection into Regioregular Poly(3-hexylthiophene) by Molecular Doping. *Appl. Phys. Lett.* **2010**, *97*, 083303.
36. Zhang, Y.; Blom, P. W. M. Electron and Hole Transport in Poly(fluorene-benzothiadiazole). *Appl. Phys. Lett.* **2011**, *98*, 143504.
37. Mihailetchi, V. D.; Wildeman, J.; Blom, P. W. M. Space-Charge Limited Photocurrent. *Phys. Rev. Lett.* **2005**, *94*, 126602.
38. He, Z. C.; Zhong, C. M.; Huang, X.; Wong, W. Y.; Wu, H. B.; Chen, L. W.; Su, S. J.; Cao, Y. Simultaneous Enhancement of Open-Circuit Voltage, Short-Circuit Current Density, and Fill Factor in Polymer Solar Cells. *Adv. Mater.* **2011**, *23*, 4636–4643.